

Ultrafast metal-to-insulator switching in a strongly correlated system

Francesco Grandi¹ and Martin Eckstein¹

¹*Department of Physics, University of Erlangen-Nürnberg, 91058 Erlangen, Germany*

(Dated: April 9, 2021)

Light-manipulation of correlated electronic phases in solids offers the tantalizing prospect of realizing electronic devices operating at the ultrafast time-scale. In this context, the experimental realization of non-equilibrium transitions from a metal to a band or Mott insulator has shown to be particularly elusive. Using dynamical mean-field theory, we study a simple model representing the main physical properties of the oxygen-enriched compound LaTiO_{3+x} . By properly optimizing the photo-doping of electrons from a low-energy band into the valence states of the system, we show it is possible to induce a valence transition from a correlated metallic state to a Mott insulator at ultrashort time scales and to contain the heating during this process, with the final non-thermal valence insulator having almost the same effective temperature of the starting metal.

I. INTRODUCTION

Transition metal compounds (TMC) are an intriguing class of materials in condensed matter physics due to the conspiracy of charge, spin, orbital and lattice degrees of freedom [1]. Many representatives of this group show a metal-to-insulator transition upon changing intensive variables such as the temperature T , the external pressure or the chemical potential [2, 3]. The equilibrium insulator-to-metal phase transition is typically realized upon increasing T if it involves some form of symmetry breaking (lattice dimerization, orbital order, antiferromagnetism, etc.) [4–7]. On the other hand, if both metal and insulator have the same symmetry, the transition to the insulator might occur with increasing instead of decreasing T , simply because the entropy of the Mott state can be higher than that of the metallic state. For example, after locking the charge, the remaining spin degree of freedom in a spin-disordered Mott insulator implies a high entropy $S_{\text{Mott}} \sim \ln(2)$ per lattice site [8]. In contrast, the entropy in a Fermi liquid vanishes for low temperatures like $S_{FL}(T) \propto T$ so that the transition to a Mott state can be driven by a temperature increase if the spin order remains frustrated.

While some of the equilibrium properties of these materials are still not fully understood, a large interest in their non-equilibrium behavior has grown recently [9, 10]. In particular, the tantalizing prospect of realizing a Mottronic switch between insulating and metallic states has attracted much attention [11–16]. Even if ultrafast insulator-to-metal phase transitions have been reported in several materials [17–21], the opposite phase change is harder to achieve. Since a laser excitation typically increases the effective temperature and the total entropy of a system, it is generally easier to move from a symmetry broken insulating state to a metallic one. Nevertheless, one can imagine several pathways to laser-induce the opposite transition from metallic to insulating behavior if the final insulating state is of the Mott kind. Firstly, with the entropic argument given above, the metal-to-insulator phase transition may be induced in some specific cases simply by a laser-induced heat-

ing of the electrons. An alternative scenario is that a photo-induced transfer of charges from other bands into a previously doped valence band can bring the latter to commensurate filling. While this will not make the system insulating as a whole (because holes are generated in other previously filled bands), Mott physics can arise in the valence band. In the following, we will term this transient state a *valence Mott insulator*. Again, the main difficulty is that a rapid charge transfer typically leads to a strong increase of the entropy, working against correlation effects. The question is, therefore, whether suitably optimized protocols can be designed to generate such a valence Mott state within short times.

Even if the entropy of the system as a whole is expected to grow after the pulse, the entropy might transiently decrease in a given subsystem, leaving the remainder at high entropy. This concept has been explored theoretically during the past years [22–25] as a pathway to induce or enhance electronic orders. Recently, it has been observed that also a charge transfer between different bands can realize this entropy redistribution [26]. By transferring (“evaporating”) holes from the valence band to localized core levels, entropy is reshuffled between the valence and the core states, with the latter having practically zero entropy before the arrival of the pulse. In [26], a single-band strongly correlated metal is considered as the initial state. By photo-doping from a narrow core level, the occupation of the valence band becomes almost commensurate with the lattice, and the effective temperature of the valence subsystem can decrease and eventually reach values below the equilibrium antiferromagnetic Néel temperature. This mechanism has therefore been termed *cooling by photo-doping*. With a similar mechanism, an enhancement of the η -paired superconducting susceptibility in the half-filled single-band Hubbard model has been predicted [27].

In this paper, we aim to investigate the cooling by photo-doping procedure in a multi-band setup. While the simulations will be based on a simplified two-band model in order to make them feasible, this model is designed to capture the important properties of the $3d^1$ perovskite series. The latter includes the metallic com-

pounds BaVO_3 , SrVO_3 , and CaVO_3 , and the Mott insulators LaTiO_3 and YTiO_3 [28–31]. In all these materials, the transition metal atoms sit at the centre of a corner-sharing O_6 octahedron, while the cations occupy the interstitial space between the octahedra. The cubic crystal field splits the 3d manifold in two higher energy e_g and three lower energy t_{2g} levels, filled with a single electron. We particularly focus on LaTiO_3 , the first insulating member of the series. In this compound, a distortion of the GdFeO_3 kind lowers the lattice symmetry to orthorhombic and further splits the t_{2g} states into a lower energy a_g level and a higher energy e'_g doublet [32]. The material has a Mott-gap of ~ 0.2 eV, which is small compared to the bandwidth of approximately $W \sim 2.1$ eV [33, 34]. A broad band, mainly derived from oxygen p-orbitals, lies well below the t_{2g} manifold [35]. Below temperature $T_N \sim 146$ K, the system undergoes a transition from a paramagnet to G-type antiferromagnetism [36].

The small value of the energy gap observed in this material suggests its proximity to a metal-insulator phase boundary, making it interesting for Motttronics [37]. Moreover, this compound shows a doping-driven phase transition by growing it under oxygen atmosphere so that the high-temperature non-stoichiometric compound LaTiO_{3+x} , with $x \sim 0.04$, is a correlated metal with well defined quasi-particle properties [34, 38–40]. In the following, we explore the possibility to drive the d-valence bands in the oxygen-enriched compound LaTiO_{3+x} from the metallic to the Mott insulating state by photo-doping electrons into the energy states around the Fermi level from the lower-energy p-derived band. In other words, the oxygen p-bands are supposed to take the role of the core bands in the cooling by photo-doping scenario, in spite of these bands being certainly not localized, but in contrast even broader than the valence bands. Depending on the form of the excitation pulse, we indeed find that the valence band state can be turned into a Mott insulator with an effective temperature almost equal to the one of the starting metal on ultrafast timescales due to an entropy increase in the oxygen bands, similar to the cooling by photo-doping protocol.

The article is organized as follows. In Sec. II, we define a minimal model for the description of the photo-doping process in LaTiO_{3+x} (Sec. II A), discuss the excitation protocol (Sec. II B) and the solution of the model using non-equilibrium dynamical mean-field theory (DMFT) (Sec. II C). In Sec. III, we present our results, showing the properties of the charge transfer process (Sec. III A) and the characteristics of the final state for several pulse lengths and optimized pulse parameters (Sec. III B). Finally, Sec. IV is devoted to concluding remarks.

II. MODEL AND METHOD

A. Two-band model

This section aims to define a minimal model that can describe the photo-induced metal-to-valence insulator transition in the oxygen-enriched strongly correlated compound LaTiO_{3+x} . As we already commented, the parent compound LaTiO_3 has the three t_{2g} -derived states (the lower energy a_g level and the e'_g doublet) at the valence filled with a single electron. Instead of three bands we consider two, where the degeneracy between the states is lifted by a crystal field interaction that mimics the effect of the GdFeO_3 -like distortion. This way, we neglect the double degeneracy of the e'_g states, which should however not alter the qualitative picture we aim to present because these states are mostly empty. Indeed, having two bands is already enough to explore the role of orbital imbalance in this system and to describe the nearly inter-band gap predicted in several theoretical analysis [30, 32]. In our two-band model, the undoped Mott insulator corresponds to quarter filling (one electron per site), and the total filling per site will be fixed to 0.92 for the doped compound. In LaTiO_{3+x} , a valence occupation 0.92 would correspond to oxygen-doping $x = 0.04$, enough for the material to show well-defined correlated metal properties.

The Hamiltonian of the two-band model is given by the sum of a local (H_{loc}) and a non-local (H_{hop}) contribution,

$$H = H_{\text{hop}} + H_{\text{loc}}. \quad (1)$$

The local part is given by

$$H_{\text{loc}} = -\frac{\Delta}{2} \sum_{\mathbf{R}} (n_{\mathbf{R},1} - n_{\mathbf{R},2}) - \mu \sum_{\mathbf{R}} n_{\mathbf{R}} + U \sum_{\mathbf{R},a} n_{\mathbf{R},a,\uparrow} n_{\mathbf{R},a,\downarrow} + U' \sum_{\mathbf{R}} n_{\mathbf{R},1} n_{\mathbf{R},2}, \quad (2)$$

where the index $a = 1, 2$ labels orbitals; although this is a simplified model, we will refer to orbital 1 and 2 as a_g and e'_g , respectively. The spin takes values $\sigma = \uparrow, \downarrow$; $n_{\mathbf{R}} = \sum_{a,\sigma} n_{\mathbf{R},a,\sigma}$ is the occupation on site \mathbf{R} , Δ is the crystal field splitting coupled to the orbital imbalance $\tau_{\mathbf{R}}^z = \frac{1}{2} (n_{\mathbf{R},1} - n_{\mathbf{R},2})$, U is the intra-band Hubbard interaction, and U' is the inter-band Hubbard repulsion. The Hund's coupling is relevant only for doubly occupied states and, moreover, is expected to be small compared to the bandwidth [41], so its contribution is neglected. The chemical potential μ is used to fix the average occupation ($n_{\mathbf{R}} = 0.92$) on each site.

The hopping part in Eq. (1) is written as

$$H_{\text{hop}} = - \sum_{\langle \mathbf{R}, \mathbf{R}' \rangle} \sum_{\sigma, a, a'} v_{\mathbf{R},a;\mathbf{R}',a'} \left(c_{\mathbf{R},a,\sigma}^\dagger c_{\mathbf{R}',a',\sigma} + \text{H.c.} \right). \quad (3)$$

The operator $c_{\mathbf{R},a,\sigma}$ ($c_{\mathbf{R},a,\sigma}^\dagger$) annihilates (creates) an electron on site \mathbf{R} in orbital a with spin σ , and the summa-

tion extends just over nearest-neighbor sites. The hopping matrix $v_{\mathbf{R},a;\mathbf{R}',a'}$ allows both intra- and inter-band charge transfers, so that the occupation of each band is not individually conserved. We take the intra-band hopping $v_{\mathbf{R},a;\mathbf{R}',a} = v/\sqrt{z}$ equal for all nearest neighbors (z is the coordination number). The inter-band hopping $v_{\mathbf{R},1;\mathbf{R}',2} = v_{\mathbf{R},2;\mathbf{R}',1}$ has absolute value v'/\sqrt{z} and phases such that

$$\sum_{\mathbf{R}'} v_{\mathbf{R},1;\mathbf{R}',2} = 0, \quad (4)$$

so that the two bands do not mix at the Γ -point. Below, we will solve the model on an infinitely-coordinated Bethe lattice, mainly because this implies a closed form of the DMFT self-consistency (as described in Sec. II C) and therefore allows to perform simulations up to longer times. It can be expected that the simulations on the Bethe lattice give qualitatively the same physics as on a cubic lattice if the bandwidth and energy gaps are properly matched and if the local environment [Eq. (4)] of every site is correctly represented.

The parameters in Eq. (1) are chosen so that the bandwidth and energy gaps are comparable to the LaTiO₃-derived compound: the energy scale is set to the half-bandwidth, which is $2v$, and time is measured in units of $\hbar/(2v)$. Because the bandwidth in LaTiO₃ is 2.1 eV [30, 32], we can almost read the energy units in our plots in electronvolts. Further, we fix the crystal field to $\Delta = 0.15$ [31, 42, 43] and the inter-band hopping $v' = 0.15$ [30]. Finally, we set the values of the intra- and inter-orbital Hubbard repulsion to $U = 3.10$ and $U' = 2.294$, respectively, to reproduce experimentally obtained energy gap of the quarter-filled (undoped) system, as well as the inter-band nature of the gap. This way, the ratio U'/U has the same value as obtained in more sophisticated calculations [42]. The initial inverse temperature of the problem is $\beta = 10$, well above the antiferromagnetic critical temperature.

Figure 1(a) shows the orbitally-resolved spectral functions of the model obtained using DMFT (Sec. II C) at $\beta = 10$. The system features a lower band of mostly a_g -character, a Hubbard gap of about 0.2, and an upper Hubbard band (UHB) which is of predominantly e'_g character at the lower edge. Upon hole-doping (Fig. 1b), a quasiparticle band is formed at the lower Hubbard band edge. In addition to the d -bands, we add an additional low-lying noninteracting band with semi-elliptic density of states, representing the p -band manifold (depicted by $A_p(\omega)$ in Fig. 1).

B. Excitation pulse

The system is excited with a time-dependent hybridization $v_{pd}(t) = AE(t)$ between the d and p bands, representing a dipolar transition driven by the electric field of a laser $E(t)$, with the dipolar matrix element A ;

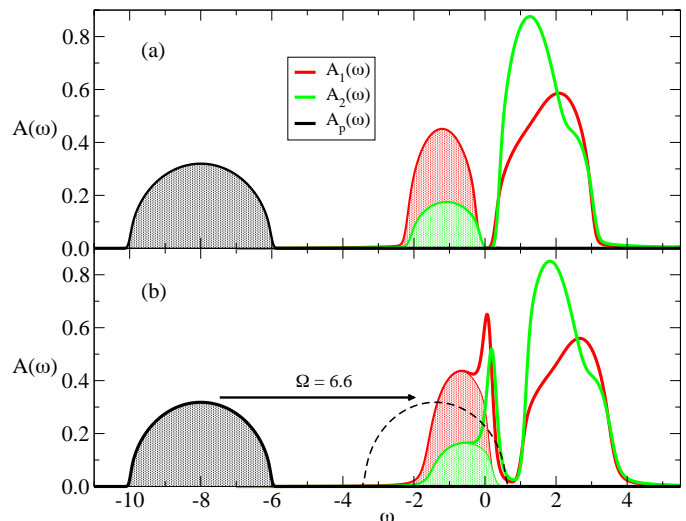


Figure 1. Spectral functions for the two orbitals $A_1(\omega)$ (red) and $A_2(\omega)$ (green), and the non-interacting p -band $A_p(\omega)$ (black), together with their occupations (shaded areas) for the undoped (panel (a)) and the doped (panel (b)) systems, where we consider an average filling per site $n = 1$ and $n = 0.92$, respectively. The effect of a finite hopping frequency Ω is to shift the fermionic bath up in energy, as schematically shown by the arrow and the dashed line in panel (b). The frequencies ω are shown with respect to the Fermi level of the system. The values of the double occupancies and of the orbital imbalance of the systems are given by $d \sim 0.0300$ and $\tau_z \sim 0.2197$ for $n = 1$, and by $d \sim 0.0234$ and $\tau_z \sim 0.2077$ for $n = 0.92$.

choosing $A = 1$ in the following sets the unit of the electric field. As in Ref. [26], we will investigate the use of chirped laser pulses [44] for controlling the system. The functional form for the electric field is taken as

$$E(t) = E_0 f_{\text{env}}(t) \sin(\Omega(t)t), \quad (5)$$

characterized by the amplitude E_0 , a linearly chirped frequency

$$\Omega(t) = \Omega_{\text{st}} + \frac{\Omega_{\text{end}} - \Omega_{\text{st}}}{t_{\text{pulse}}} t \quad (6)$$

with pulse duration t_{pulse} and start (end) frequency Ω_{st} (Ω_{end}), and a smooth envelope of duration t_{pulse} , $f_{\text{env}}(t) = [(1 + e^{\alpha(t-t_{\text{pulse}})+6})(1 + e^{-\alpha t+6})]^{-1}$. In the following, we consider pulses with different durations t_{pulse} , and optimize all parameters α , E_0 , Ω_{st} and Ω_{end} to achieve certain final states (Sec. III).

C. DMFT solution

We solve the model using nonequilibrium DMFT [8, 45, 46]. In DMFT, the original Hamiltonian Eq. (1) is mapped onto a single-site impurity with local properties that correspond to Eq. (2). The impurity is hybridized with a bath characterized by a self-consistent

hybridization matrix $\Delta_{a,b}(t,t')$, with orbital indexes a, b . Because we consider relatively high temperatures and interaction strengths, we can to first approximation apply the non-crossing approximation (NCA) as impurity solver [47]. Our choice of the hopping matrix in Eq. (3), and in particular the condition in Eq. (4), allows to solve the problem entirely in terms of the diagonal components $\Delta_a(t,t') = \Delta_{a,a}(t,t')$ of the hybridization matrix. On the Bethe lattice, the self-consistency relation takes a closed form,

$$\Delta_a(t,t') = v^2 G_a(t,t') + v'^2 G_{\bar{a}}(t,t') + \Delta_p(t,t') , \quad (7)$$

where $G_a(t,t')$ is the local contour-ordered electronic Green's function for band a , $\bar{a} = 2$ for $a = 1$ and vice versa, and $\Delta_p(t,t')$ is the hybridization function due to the coupling of the valence bands to the non-interacting p -band. The latter is given by

$$\Delta_p(t,t') = v_{pd}(t) G_p^0(t,t') v_{pd}(t') , \quad (8)$$

where $G_p^0(t,t')$ is the local Green's function of the p -band (with a semi-elliptic density of states of bandwidth 4, as shown in Fig. 1), and $v_{pd} = E(t)$ is the field-controlled inter-band hybridization. The time-dependent spectral and occupation functions are computed from the retarded and lesser components of the Green's functions via backward Fourier transformation:

$$\begin{aligned} A_a(\omega, t) &= -\frac{1}{\pi} \text{Im} \int_0^{s_{\max}} ds G_a^R(t, t-s) e^{-i\omega s} , \\ A_a^<(\omega, t) &= \frac{1}{\pi} \text{Im} \int_0^{s_{\max}} ds G_a^<(t, t-s) e^{-i\omega s} . \end{aligned} \quad (9)$$

The total spectral function is defined as the sum, $A(\omega, t) = A_1(\omega, t) + A_2(\omega, t)$, and similarly for $A^<(\omega, t)$.

III. RESULTS

A. Time-dependent charge transfer

In this section, we present the results obtained by solving the model Eq. (1) using nonequilibrium DMFT, starting from the equilibrium configuration depicted in Fig. 1(b). The dipolar coupling of the valence bands with the p -band has the net effect of increasing the filling of the valence bands, see Fig. 2(a). Since our main aim is to induce a metal-to-Mott insulator phase transition in the valence bands, we target the nearest commensurate filling of the valence bands, $n = 1$. By applying laser pulses of different durations, we realize that the dynamics of n can be divided essentially into two steps: (i) A growth from the initial value $n \sim 0.92$ to an occupation $n > 1$ larger than the target one, and then (ii), a convergence of n to the desired occupation $n \sim 1$, see Fig. 2(a). The maximum value of the occupation reached during the dynamics is higher for shorter pulses. In passing, we note that each pulse is tailored to minimize the occupation of

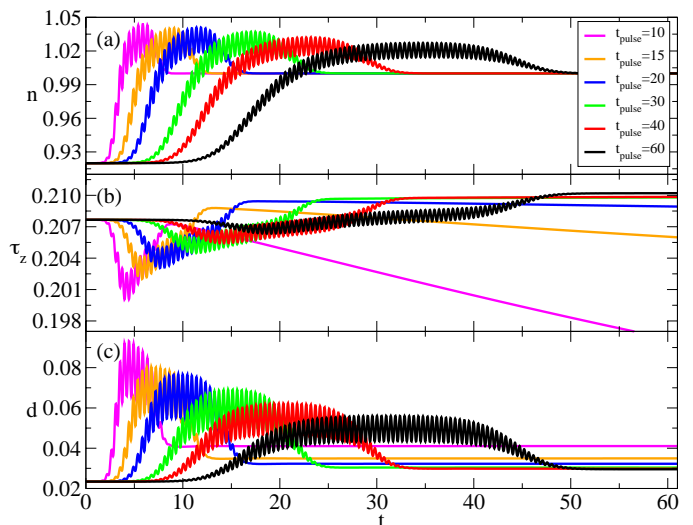


Figure 2. Time dependence of the occupation per site $n = n_1 + n_2$ (panel (a)), of the orbital imbalance τ_z (panel (b)) and of the double occupation d (panel (c)) for several pulse durations t_{pulse} . Each pulse is tailored to minimize the occupation of the UHBs in the final state.

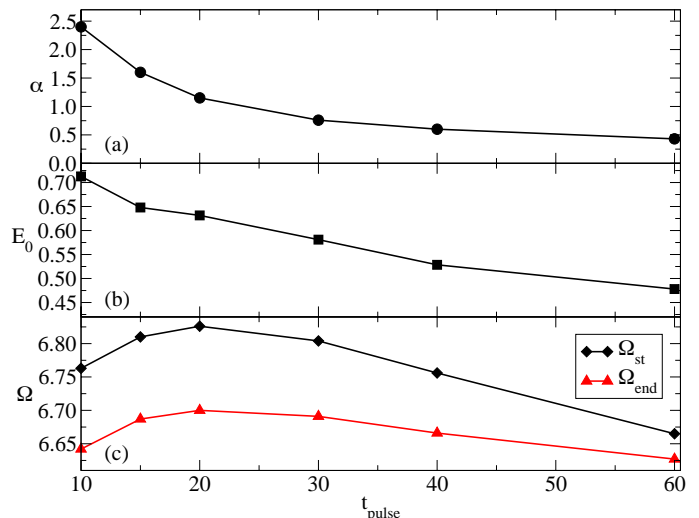


Figure 3. Optimized pulse parameters α (panel (a)), E_0 (panel (b)) and Ω_{\min} , Ω_{\max} (panel (c)) as a function of the pulse duration t_{pulse} , for the pulses used in the simulations shown in Fig. 2.

the UHBs in the final state. The resulting pulse parameters for the pulses used in Fig. 2 are shown in Fig. 3, while the optimization procedure is described in Sec. III B.

Once the p -band is decoupled from the valence bands, the number of electrons in the valence bands stays fixed because direct charge transfer processes are activated only in the presence of the electric field. Other recombination channels, which are not included in the model, should be weak in the real material and therefore not relevant on the timescale of the present study. In partic-

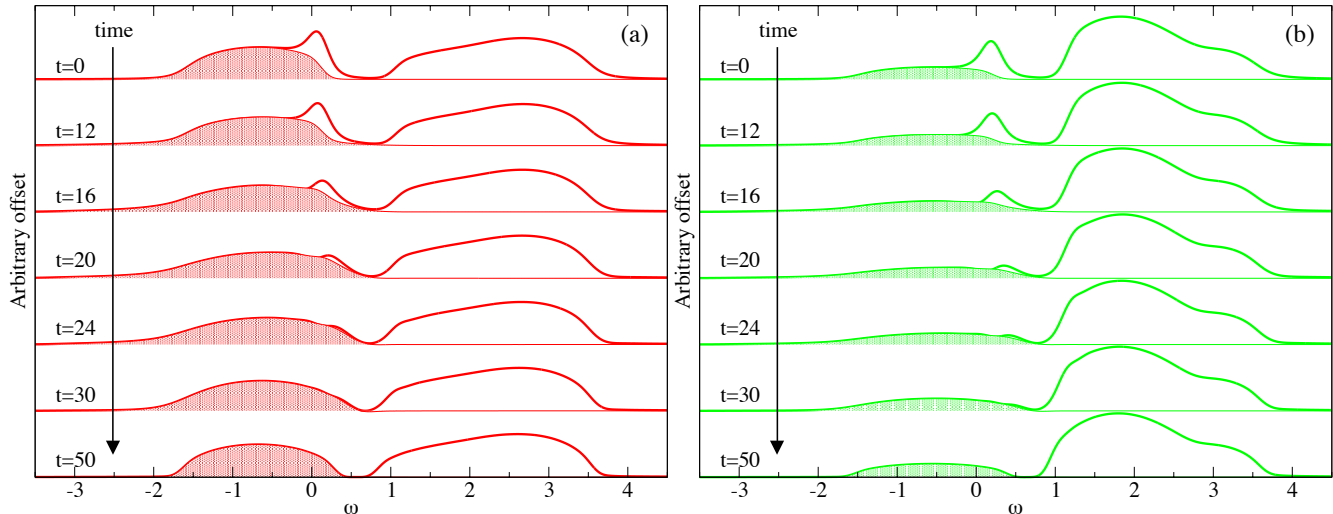


Figure 4. Panel (a): spectral functions (lines) of band 1 at different times and respective occupations (shaded areas) during and after the pulse with $t_{\text{pulse}} = 40$ analyzed in Fig. 2. Panel (b): same as for panel (a), but for band 2. The starting time for the simulations in this figures is $t = -30$, and the pulse arrives at $t = 0$.

ular, the main recombination channels would be either phonon-assisted, which is slow because of the large energy mismatch between phonons and the p-d energy separation, and p-d electron-electron scattering, which is weak if the p-hole and the photodoped electron are mainly located on different atoms (oxygen and titanium).

The double occupation d shows qualitatively similar dynamics as the density, see Fig. 2(c). The final value of d decreases for longer pulses, suggesting a final state with a smaller number of excitations. Finally, the charge distribution of the model is also characterized by the orbital imbalance τ^z , shown in Fig. 2(b). At earlier times, τ^z changes roughly opposite to the total occupation: When n increases, τ^z decreases and vice versa. After the pulse, the orbital imbalance continues to decrease, in particular after the shorter pulses $t_{\text{pulse}} = 10, 15, 20$, indicating inter valence-band thermalization processes.

To get more insight into what happens during the dynamics, we show in Fig. 4 some snapshots of the spectral functions of the valence bands during one of the longer pulses considered in Fig. 2. The quasiparticle peaks of the two bands observed in equilibrium are gradually suppressed, and entirely vanish once the pulse is over. Thus, while at the initial stage of the dynamics the system is in a correlated metallic state, after the photo-doping the system reaches a Mott state. As seen in Fig. 1, the initial metallic state already shows a preformed Mott gap within the unoccupied region of the spectrum. This gap is reduced at intermediate stages of the dynamics due to the hybridization of the valence with the lower energy band (see the intermediate spectral functions shown in Fig. 4). In the final state, a well-defined Mott gap is restored.

B. Final state and pulse optimization

Following the original aim of transferring the valence bands into a Mott state, we now analyze the final state after the pulse as a function of the pulse parameters. The insulating character of the state after the pulse strongly depends on the pulse duration t_{pulse} . Figures 5(a) and (b) show the spectral functions of the Mott insulators reached after pulses of duration $t_{\text{pulse}} = 10$ and $t_{\text{pulse}} = 40$, respectively. It becomes apparent that for the shorter pulse, the final state looks like a Mott insulator with both occupation in the UHB and hole occupation in the lower Hubbard band (LHB), and still some signatures of metallic character such as quasiparticle peaks in particular on the upper edge of the lower Hubbard band. This state can be called a photo-doped Mott-insulator [48]. In contrast, for the longer pulse, the final insulating state resembles a low-temperature Mott insulator.

One could attempt to extract an effective temperature of these states (and also for the transient states) by analyzing the distribution function $F(\omega, t) = \frac{A^<(\omega, t)}{A(\omega, t)}$ in terms of a Fermi-Dirac fit with a given inverse temperature $\beta_{\text{eff}}(t)$. This would also tell if an effective temperature is well-defined during the dynamics, i.e., whether the laser induced charge transfer can be viewed as an adiabatic process. However, even for the longer pulses, we find a substantial mismatch between the time-dependent distribution function and the Fermi-Dirac distribution during the pulse. Also after the pulse, a Fermi-Dirac fit is difficult: for shorter pulses, the simultaneous hole occupation in the LHB and electron occupation in the UHB (as in Fig. 5a) does not fit a Fermi distribution, while for longer pulses, where the system becomes closer to a low-temperature Mott insulating state, a Fermi-Dirac fit

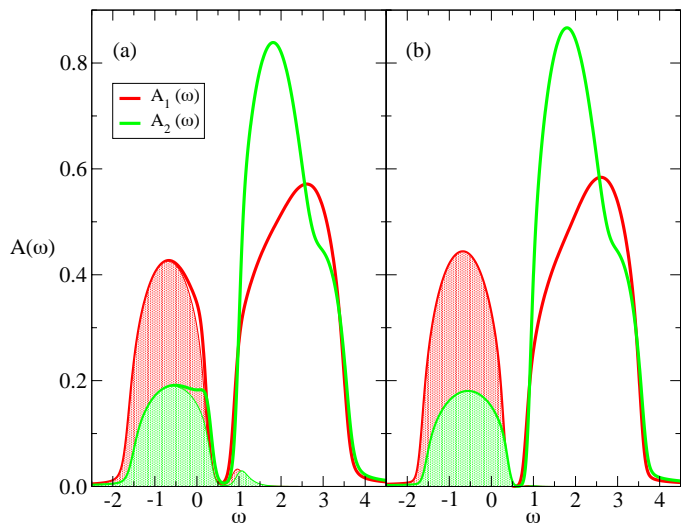


Figure 5. Spectral functions for the two orbitals $A_1(\omega)$ (red) and $A_2(\omega)$ (green), and respective occupations (shaded areas) computed by a backward Fourier transformation at time $t = 130$ after the pulses $t_{\text{pulse}} = 10$ (panel (a)) and $t_{\text{pulse}} = 40$ (panel (b)) analyzed in Fig. 2.

is not possible simply because a distribution cannot be properly defined in the region of the gap and is either zero or unity outside.

We therefore proceed by characterizing the final state in terms of its energy. We compare the state of the system with a thermal state sharing the same internal energy and a total valence occupation $n = 1$. The inverse temperature β_{eff} of this equilibrium reference state is shown in Fig. 6(a). We can distinguish two main regimes here: When the pulse is short, the effective temperature of the system is increased with respect to the temperature of the initial equilibrium system $\beta = 10$, while with longer pulses there is the possibility to at least keep the effective temperature close to the initial value. Essentially, we have a transition from a regime where the effect of the laser pulse is to produce a photo-doped Mott insulator to a range where the entropy increase in the valence bands remains controlled, as in the cooling by photo-doping protocol. The red squares shown in Fig. 6(c) and (d) represent the values of the orbital imbalance and the double occupation, respectively, as a function of the pulse duration obtained from the equilibrium reference state with the inverse temperatures shown in Fig. 6(a). The black circles in Fig. 6(c) and (d) are instead the values of τ_z and d at the end of the total simulation time for the curves shown in Fig. 2(b) and (c). The crossing of the curves around $t_{\text{pulse}} \sim 30$ separates two regimes: Below $t_{\text{pulse}} \sim 30$, the system looks warmer than the corresponding equilibrium state if we look at the double occupation, while it appears colder if we look at the orbital imbalance; above $t_{\text{pulse}} \sim 30$, the opposite behavior occurs. While the double occupation is essentially constant in the state reached once the pulse is over, see

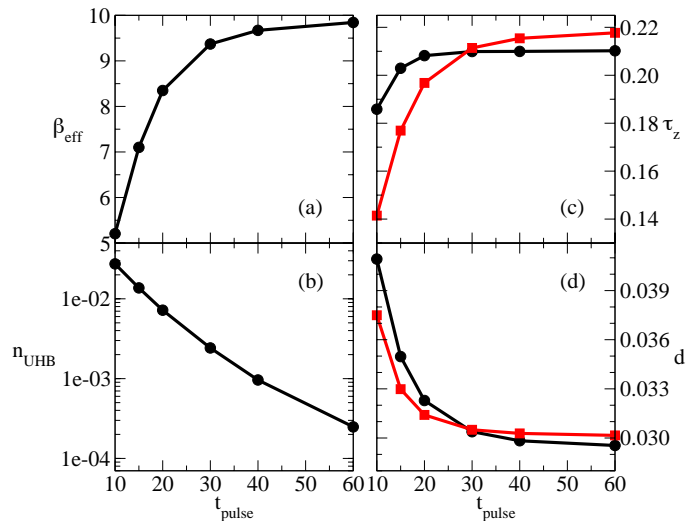


Figure 6. (a) Effective inverse temperature β_{eff} of the system after the action of a time dependent pulse of duration t_{pulse} . The inverse temperature is computed by looking at the internal energy of the system after the pulse. (b) Occupation of the upper Hubbard band as a function of the duration of the pulse t_{pulse} . Panel (c) and (d): orbital imbalance and double occupation of the system, respectively, at the latest time of our simulations (circles) and in an equilibrium state with the same temperature as in panel (a) (squares).

Fig. 2(c), the orbital imbalance evolves towards the corresponding equilibrium value. Thus it keeps decreasing for short pulses (characterized by $t_{\text{pulse}} \leq 20$), and slowly increasing for longer pulses, see Fig. 2(b).

As expected, different pulse shapes Eq. (5) lead to different final states. To choose the specific form of the laser pulse in the simulations so far, we optimized the parameters Ω_{end} , Ω_{st} , α , and E_0 for each pulse duration t_{pulse} , keeping the final occupation $n = 1$ fixed. For the optimization, we start using Eq. (5) for a non-chirped pulse close to $\Omega_{\text{end}} = \Omega_{\text{st}} = \Omega \sim 6.65$ (set by the p-d splitting) and $\alpha \sim 1$, and determine E_0 to impose the desired total occupation $n \sim 1$. Considering several values of Ω , we find the configuration that minimizes the occupation of the UHB at given α . Repeating this procedure for several values α , we optimize the number of excitations in the system for this parameter too. Once we are in the best possible state according to our requirements, we allow Ω_{end} to be different from Ω_{st} , permitting us to optimize the excitations number respect to the unchirped configuration slightly. (Certainly an automatic multi-parameter pulse optimization based on machine learning techniques would be intriguing, but computationally costly due to the potentially large number of simulations required in the optimization.) The optimized parameters are shown in Fig. 3. The optimal pulse shape is indeed found to be slightly chirped, with Ω_{end} smaller than Ω_{st} , and a chirping amplitude $\Delta\Omega_{\text{ch.}} = \Omega_{\text{st}} - \Omega_{\text{end}}$ comparable to the gap size, see Fig. 3(c). Figure. 7 shows the occupation of the UHB n_{UHB} against $\Delta\Omega_{\text{ch.}}$ for pulses characterized

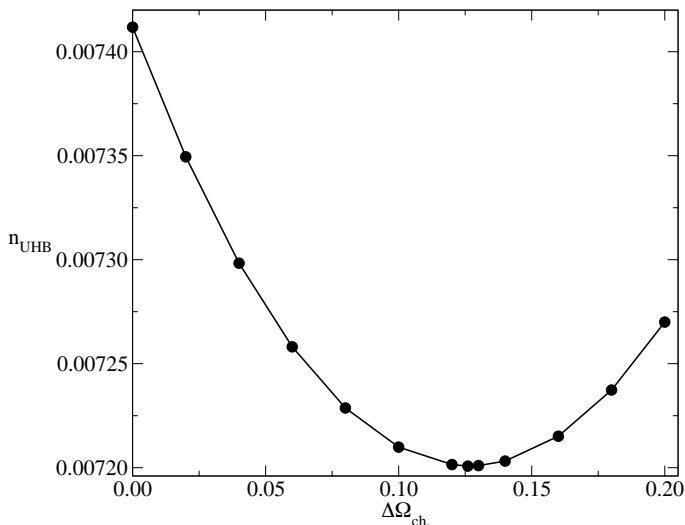


Figure 7. Occupation of the UHB as a function of the chirping amplitude $\Delta\Omega_{\text{ch}}$, for pulses with $t_{\text{pulse}} = 20$, $\alpha = 1.15$ and $\Omega_{\text{end}} = 6.700$.

by $t_{\text{pulse}} = 20$, $\alpha = 1.15$ and $\Omega_{\text{end}} = 6.700$. Each point in Fig. 7 is computed at a different amplitude E_0 to impose the total occupation of the final state $n \sim 1$. The minimum of n_{UHB} occurs at $\Delta\Omega_{\text{ch}} = 0.126$, corresponding to $\Omega_{\text{st}} = 6.826$, as reported in Fig. 3(c).

A final question we would like to address is at which speed the transition from the metallic to the Mott insulating regime can be achieved. Since we target to keep a small number of excitations, we plot the number of electrons in the UHB once the pulse is over as a function of the pulse duration, as shown in Fig. 6(b). Not surprisingly, the shorter the pulse, the higher the number of excitations in the system. We expect the curve to follow the exponential decay $Ce^{-E_g^{\text{fit}}t_{\text{pulse}}}$, where E_g^{fit} should be of the order of the bandgap E_g for the best possible pulse process. By fitting the curve Fig. 6(b) with the exponential function, we obtain $C \sim 0.102$ and $E_g^{\text{fit}} \sim 0.132$, with the second parameter of the same order of magnitude of the gap size $E_g \sim 0.2$. We notice that, while the three points at $t_{\text{pulse}} \leq 20$ in Fig. 6(b) are well fitted, the last three depart from the fitting line. For this, one also must keep in mind that the exponentially small excitation densities become increasingly difficult to measure numerically. The decrease in n_{UHB} observed in Fig. 6(b)

over several order of magnitudes indicates what should be the approximate pulse length to get the desired number of excitations in the system.

IV. CONCLUSIONS

In this study, we analyzed the possibility to induce an ultrafast metal-to-valence Mott insulator transition in a model system relevant to the physics of the oxygen-enriched transition metal compound LaTiO_{3+x} . Through non-equilibrium dynamical mean-field theory (with the non-crossing approximation as an impurity solver), we considered the effect of the dipolar photo-doping of electrons from a core state representative of the broad p-derived oxygen band to the valence states that mimic the t_{2g} manifold at the Fermi level. An external laser pulse opens a charge transfer channel from the oxygen related bands to the valence bands. At each given pulse duration, we optimized the shape of the pulse to reach the desired final occupation and simultaneously minimize the number of excitations in the upper Hubbard bands. Depending on the pulse length, we get a crossover from a regime where the final state is a Mott insulator characterized by an effective temperature almost equal to the one of the initial correlated metallic system to a regime where this effective temperature is substantially larger. The crossover is at pulse durations as short as 30 hopping times.

Although the model under investigation is highly simplified, this suggests that a photo-induced charge transfer to a valence Mott-insulator can be realized in LaTiO_{3+x} on the 100 fs timescale without substantially heating the system. As in the cooling by photo-doping mechanism, the limited heating can be related to the fact that a large amount of entropy is stored in the oxygen related bands after the photo-induced charge transfer.

ACKNOWLEDGEMENTS

We thank Philipp Werner for useful discussions. This work was supported by the ERC starting grant No. 716648. The authors gratefully acknowledge the computational resources and support provided by the Erlangen Regional Computing Center (RRZE).

-
- [1] Daniel I. Khomskii, *Transition Metal Compounds* (Cambridge University Press, 2014).
 [2] F. J. Morin, “Oxides which show a metal-to-insulator transition at the neel temperature,” *Phys. Rev. Lett.* **3**, 34–36 (1959).
 [3] Masatoshi Imada, Atsushi Fujimori, and Yoshinori Tokura, “Metal-insulator transitions,” *Rev. Mod. Phys.* **70**, 1039–1263 (1998).

- [4] J. B. Torrance, P. Lacorre, A. I. Nazzari, E. J. Ansaldo, and Ch. Niedermayer, “Systematic study of insulator-metal transitions in perovskites RNiO_3 (R=Pr,Nd,Sm,Eu) due to closing of charge-transfer gap,” *Phys. Rev. B* **45**, 8209–8212 (1992).
 [5] D. B. McWhan, A. Menth, J. P. Remeika, W. F. Brinkman, and T. M. Rice, “Metal-Insulator Transitions in Pure and Doped V_2O_3 ,” *Phys. Rev. B* **7**, 1920–1931

- (1973).
- [6] J. H. Park, J. M. Coy, T. S. Kasirga, C. Huang, Z. Fei, S. Hunter, and D. H. Cobden, “Measurement of a solid-state triple point at the metal-insulator transition in VO_2 ,” *Nature* **500**, 431 (2013).
- [7] Benjamin A. Frandsen, Lian Liu, Sky C. Cheung, Zurab Guguchia, Rustem Khasanov, Elvezio Morenzoni, Timothy J. S. Munsie, Alannah M. Hallas, Murray N. Wilson, Yipeng Cai, Graeme M. Luke, Bijuan Chen, Wenmin Li, Changqing Jin, Cui Ding, Shengli Guo, Fanlong Ning, Takashi U. Ito, Wataru Higemoto, Simon J. L. Billinge, Shoya Sakamoto, Atsushi Fujimori, Taito Murakami, Hiroshi Kageyama, Jose Antonio Alonso, Gabriel Kotliar, Masatoshi Imada, and Yasutomo J. Uemura, “Volume-wise destruction of the antiferromagnetic Mott insulating state through quantum tuning,” *Nature Communications* **7**, 12519 (2016).
- [8] Antoine Georges, Gabriel Kotliar, Werner Krauth, and Marcelo J. Rozenberg, “Dynamical mean-field theory of strongly correlated fermion systems and the limit of infinite dimensions,” *Rev. Mod. Phys.* **68**, 13–125 (1996).
- [9] Claudio Giannetti, Massimo Capone, Daniele Fausti, Michele Fabrizio, Fulvio Parmigiani, and Dragan Mihailovic, “Ultrafast optical spectroscopy of strongly correlated materials and high-temperature superconductors: a non-equilibrium approach,” *Advances in Physics* **65**, 58–238 (2016).
- [10] D. N. Basov, R. D. Averitt, and D. Hsieh, “Towards properties on demand in quantum materials,” *Nature Materials* **16**, 1077–1088 (2017).
- [11] V. Guiot, L. Cario, E. Janod, B. Corraze, V. Ta Phuoc, M. Rozenberg, P. Stoliar, T. Cren, and D. Roditchev, “Avalanche breakdown in $\text{GaTa}_4\text{Se}_{8-x}\text{Te}_x$ narrow-gap Mott insulators,” *Nature Communications* **4**, 1722 (2013).
- [12] G. Mazza, A. Amaricci, M. Capone, and M. Fabrizio, “Field-Driven Mott Gap Collapse and Resistive Switch in Correlated Insulators,” *Phys. Rev. Lett.* **117**, 176401 (2016).
- [13] Jiajun Li, Camille Aron, Gabriel Kotliar, and Jong E. Han, “Microscopic theory of resistive switching in ordered insulators: Electronic versus thermal mechanisms,” *Nano Letters* **17**, 2994–2998 (2017).
- [14] Andrea Ronchi, Paolo Franceschini, Pia Homm, Marco Gandolfi, Gabriele Ferrini, Stefania Pagliara, Francesco Banfi, Mariela Menghini, Jean-Pierre Locquet, and Claudio Giannetti, “Non-thermal light-assisted resistance collapse in a V_2O_3 -based Motronic device,” (2020), [arXiv:2012.15255 \[cond-mat.str-el\]](https://arxiv.org/abs/2012.15255).
- [15] Javier del Valle, Pavel Salev, Federico Tesler, Nicolás M. Vargas, Yoav Kalcheim, Paul Wang, Juan Trastoy, Min-Han Lee, George Kassabian, Juan Gabriel Ramírez, Marcelo J. Rozenberg, and Ivan K. Schuller, “Subthreshold firing in Mott nanodevices,” *Nature* **569**, 388–392 (2019).
- [16] Etienne Janod, Julien Tranchant, Benoit Corraze, Madec Querré, Pablo Stoliar, Marcelo Rozenberg, Tristan Cren, Dimitri Roditchev, Vinh Ta Phuoc, Marie-Paule Besland, and Laurent Cario, “Resistive Switching in Mott Insulators and Correlated Systems,” *Advanced Functional Materials* **25**, 6287–6305 (2015).
- [17] A. Cavalleri, Th. Dekorsy, H. H. W. Chong, J. C. Kieffer, and R. W. Schoenlein, “Evidence for a structurally-driven insulator-to-metal transition in VO_2 : A view from the ultrafast timescale,” *Phys. Rev. B* **70**, 161102 (2004).
- [18] L. Stojchevska, I. Vaskivskiy, T. Mertelj, P. Kusar, D. Svetin, S. Brazovskii, and D. Mihailovic, “Ultrafast switching to a stable hidden quantum state in an electronic crystal,” *Science* **344**, 177–180 (2014).
- [19] Daniel Wegkamp, Marc Herzog, Lede Xian, Matteo Gatti, Pierluigi Cudazzo, Christina L. McGahan, Robert E. Marvel, Richard F. Haglund, Angel Rubio, Martin Wolf, and Julia Stähler, “Instantaneous Band Gap Collapse in Photoexcited Monoclinic VO_2 due to Photocarrier Doping,” *Phys. Rev. Lett.* **113**, 216401 (2014).
- [20] G. Lantz, B. Mansart, D. Grieger, D. Boschetto, N. Nilforoushan, E. Papalazarou, N. Moisan, L. Perfetti, V. L. R. Jacques, D. Le Bolloc’h, C. Laulhé, S. Ravy, J-P Rueff, T. E. Glover, M. P. Hertlein, Z. Hussain, S. Song, M. Chollet, M. Fabrizio, and M. Marsi, “Ultrafast evolution and transient phases of a prototype out-of-equilibrium Mott-Hubbard material,” *Nature Communications* **8**, 13917 (2017).
- [21] Ia. A. Mogunov, F. Fernández, S. Lysenko, A.J. Kent, A.V. Scherbakov, A.M. Kalashnikova, and A.V. Akimov, “Ultrafast Insulator-Metal Transition in VO_2 Nanostructures Assisted by Picosecond Strain Pulses,” *Phys. Rev. Applied* **11**, 014054 (2019).
- [22] S. J. Denny, S. R. Clark, Y. Laplace, A. Cavalleri, and D. Jaksch, “Proposed parametric cooling of bilayer cuprate superconductors by terahertz excitation,” *Phys. Rev. Lett.* **114**, 137001 (2015).
- [23] Andrea Nava, Claudio Giannetti, Antoine Georges, Erio Tosatti, and Michele Fabrizio, “Cooling quasiparticles in A_3C_{60} fullerides by excitonic mid-infrared absorption,” *Nature Physics* **14**, 154 (2018).
- [24] Michele Fabrizio, “Selective transient cooling by impulse perturbations in a simple toy model,” *Phys. Rev. Lett.* **120**, 220601 (2018).
- [25] Philipp Werner and Yuta Murakami, “Nonthermal excitonic condensation near a spin-state transition,” *Phys. Rev. B* **102**, 241103 (2020).
- [26] Philipp Werner, Martin Eckstein, Markus Müller, and Gil Refael, “Light-induced evaporative cooling of holes in the Hubbard model,” *Nature Communications* **10**, 5556 (2019).
- [27] Jiajun Li, Denis Golez, Philipp Werner, and Martin Eckstein, “ η -paired superconducting hidden phase in photodoped mott insulators,” *Phys. Rev. B* **102**, 165136 (2020).
- [28] Kousuke Nishimura, Ikuya Yamada, Kengo Oka, Yuichi Shimakawa, and Masaki Azuma, “High-pressure synthesis of BaVO_3 : A new cubic perovskite,” *Journal of Physics and Chemistry of Solids* **75**, 710 – 712 (2014).
- [29] V.V. Bannikov, “Elastic, electronic and magnetic properties of new oxide perovskite BaVO_3 : A first-principles study,” *Materials Chemistry and Physics* **171**, 119 – 125 (2016).
- [30] E Pavarini, A Yamasaki, J Nuss, and O K Andersen, “How chemistry controls electron localization in $3d^1$ perovskites: a Wannier-function study,” *New Journal of Physics* **7**, 188–188 (2005).
- [31] E. Pavarini, S. Biermann, A. Poteryaev, A. I. Lichtenstein, A. Georges, and O. K. Andersen, “Mott transition and suppression of orbital fluctuations in orthorhombic $3d^1$ perovskites,” *Phys. Rev. Lett.* **92**, 176403 (2004).

- [32] H. Ishida and A. Liebsch, “Origin of metallicity of $\text{LaTiO}_3/\text{SrTiO}_3$ heterostructures,” *Phys. Rev. B* **77**, 115350 (2008).
- [33] T. Arima, Y. Tokura, and J. B. Torrance, “Variation of optical gaps in perovskite-type 3d transition-metal oxides,” *Phys. Rev. B* **48**, 17006–17009 (1993).
- [34] Y. Okimoto, T. Katsufuji, Y. Okada, T. Arima, and Y. Tokura, “Optical spectra in $(\text{La},\text{Y})\text{TiO}_3$: Variation of Mott-Hubbard gap features with change of electron correlation and band filling,” *Phys. Rev. B* **51**, 9581–9588 (1995).
- [35] Fedwa El-Mellouhi, Edward N. Brothers, Melissa J. Lucero, Ireneusz W. Bulik, and Gustavo E. Scuseria, “Structural phase transitions of the metal oxide perovskites SrTiO_3 , LaAlO_3 , and LaTiO_3 studied with a screened hybrid functional,” *Phys. Rev. B* **87**, 035107 (2013).
- [36] A. C. Komarek, H. Roth, M. Cwik, W.-D. Stein, J. Baier, M. Kriener, F. Bourée, T. Lorenz, and M. Braden, “Magnetoelastic coupling in $R\text{TiO}_3$ ($R = \text{La}, \text{Nd}, \text{Sm}, \text{Gd}, \text{Y}$) investigated with diffraction techniques and thermal expansion measurements,” *Phys. Rev. B* **75**, 224402 (2007).
- [37] M. Kubota, H. Nakao, Y. Murakami, Y. Taguchi, M. Iwama, and Y. Tokura, “Orbital ordering near a Mott transition: Resonant x-ray scattering study of the perovskite Ti oxides $R\text{TiO}_3$ and $\text{LaTiO}_{3.02}$ ($R = \text{Gd}, \text{Sm}, \text{Nd}, \text{and La}$),” *Phys. Rev. B* **70**, 245125 (2004).
- [38] Philipp Scheiderer, Matthias Schmitt, Judith Gabel, Michael Zapf, Martin Stübinger, Philipp Schütz, Lenart Dudy, Christoph Schlueter, Tien-Lin Lee, Michael Sing, and Ralph Claessen, “Tailoring Materials for Motttronics: Excess Oxygen Doping of a Prototypical Mott Insulator,” *Advanced Materials* **30**, 1706708 (2018).
- [39] Y. Taguchi, T. Okuda, M. Ohashi, C. Murayama, N. Môri, Y. Iye, and Y. Tokura, “Critical behavior in $\text{LaTiO}_{3+\delta/2}$ in the vicinity of antiferromagnetic instability,” *Phys. Rev. B* **59**, 7917–7924 (1999).
- [40] F. Lichtenberg, D. Widmer, J. G. Bednorz, T. Williams, and A. Reller, “Phase diagram of LaTiO_x : from 2D layered ferroelectric insulator to 3D weak ferromagnetic semiconductor,” *Zeitschrift für Physik B Condensed Matter* **82**, 211–216 (1991).
- [41] F. Grandi, A. Amaricci, and M. Fabrizio, “Unraveling the Mott-Peierls intrigue in vanadium dioxide,” *Phys. Rev. Research* **2**, 013298 (2020).
- [42] M. W. Haverkort, Z. Hu, A. Tanaka, G. Ghiringhelli, H. Roth, M. Cwik, T. Lorenz, C. Schüßler-Langeheine, S. V. Streltsov, A. S. Mylnikova, V. I. Anisimov, C. de Nadai, N. B. Brookes, H. H. Hsieh, H.-J. Lin, C. T. Chen, T. Mizokawa, Y. Taguchi, Y. Tokura, D. I. Khomskii, and L. H. Tjeng, “Determination of the Orbital Moment and Crystal-Field Splitting in LaTiO_3 ,” *Phys. Rev. Lett.* **94**, 056401 (2005).
- [43] Gabriele Scлаuzero, Krzysztof Dymkowski, and Claude Ederer, “Tuning the metal-insulator transition in d^1 and d^2 perovskites by epitaxial strain: A first-principles-based study,” *Phys. Rev. B* **94**, 245109 (2016).
- [44] Donna Strickland and Gerard Mourou, “Compression of amplified chirped optical pulses,” *Optics Communications* **56**, 219 – 221 (1985).
- [45] Hideo Aoki, Naoto Tsuji, Martin Eckstein, Marcus Kollar, Takashi Oka, and Philipp Werner, “Nonequilibrium dynamical mean-field theory and its applications,” *Reviews of Modern Physics* **86**, 779–837 (2014).
- [46] Michael Schüler, Denis Golež, Yuta Murakami, Nikolaj Bittner, Andreas Herrmann, Hugo U.R. Strand, Philipp Werner, and Martin Eckstein, “NESSi: The Non-Equilibrium Systems Simulation package,” *Computer Physics Communications* **257**, 107484 (2020).
- [47] Martin Eckstein and Philipp Werner, “Nonequilibrium dynamical mean-field calculations based on the noncrossing approximation and its generalizations,” *Phys. Rev. B* **82**, 115115 (2010).
- [48] Nagamalleswararao Dasari, Jiajun Li, Philipp Werner, and Martin Eckstein, “A photo-induced strange metal with electron and hole quasi-particles,” (2020), [arXiv:2010.04095 \[cond-mat.str-el\]](https://arxiv.org/abs/2010.04095).